INVESTIGATION OF A THERMAL BUOYANCY EFFECT ON THE DRAG OF HALF MODELS TESTED IN THE ARA TRANSONIC WIND TUNNEL

D R Stanniland, I F Burns, J E Green
Aircraft Research Association Ltd,
Bedford, England

Abstract

The demand for improved drag repeatability from wind tunnel measurements, together with the increasing size of models (driven by the requirement for accurate representation of small components), has led to the need for a greater understanding of the flow near the porous walls of the ARA Transonic Wind Tunnel and the implications of very small changes in this flow on the model force measurements. A detailed investigation of the variability of drag measurements on a half model identified a diurnal variation which could be attributed to the small changes in temperature difference between the tunnel shell and the freestream. This paper describes measurements which have been made in the tunnel to identify the cause of this non-repeatability. The results show a variation in the boundary layer development on the tunnel walls caused by differences in the heat transfer in the plenum chamber. This can change the Mach number in the vicinity of a half model afterbody by approximately 0.002 for a temperature increment of 5°K, implying a change in drag coefficient of 0.0002 for a typical civil aircraft model. An extension to the test section has been designed, which was successful in removing the thermal influence on the boundary layer thickness and centreline Mach number in the empty tunnel. However, some thermal buoyancy remains when a half model is tested in the redesigned section, although this is significantly reduced for a large model. A correction procedure has been developed which has virtually eliminated thermal buoyancy as a source of error, resulting in a drag repeatability of better than 1 count.

1 Introduction

Half model testing forms an important part of the workload of the ARA Transonic Wind Tunnel (TWT). It is used primarily for transport aircraft testing as a means of obtaining propulsion installation effects, using either through-flow nacelles or turbine-powered simulators, and to investigate detailed design modifications to small components such as winglets, pylons and flap-track fairings. The requirement for accurate representation of these components inevitably means that the half models are made as large as possible. In order to measure the incremental differences due to these small changes in configuration, it is necessary to discriminate very small changes in the aerodynamic forces on the model and this is only possible with a high standard of repeatability within a given test series. During the 1980s ARA developed a technique for half model testing which gave a drag repeatability within a given test series of approximately one count ($\Delta C_D \equiv 0.0001$) for a typical transport aircraft.

Early in 1990 it became apparent that the accepted drag standard was no longer being achieved, with repeat tests on a given configuration showing a variation of 2-3 drag counts. A detailed investigation was therefore implemented to re-establish the standard. This identified the main contribution to the non-repeatability as a small hysteresis in the axial force measured by the sensitive half model balance which was normally used for drag investigations. However, during the course of this investigation a diurnal variation in drag was also identified. Initially, it was thought that this could be attributed to a thermal effect on the balance measurements. Although the body of the balance was maintained at constant temperature to minimise any thermal drifts in the balance readings, it was possible that the joint between the model and the balance transmitted strain into the balance flexures as the temperature of the model increased through the day. A finite element analysis of the structure indicated that, although temperature gradients would occur in the upper part of the balance, there would be no measurable thermal strain in the axial force flexures.

In parallel with the investigation of the balance readings, pressure measurements were also made on the afterbody of a model and the tunnel walls in an attempt to identify an aerodynamic cause of the diurnal drag variation. Since a drag increment of 1 count results from a change in afterbody pressure coefficient of 0.001 for a typical transport aircraft configuration, it was apparent that extreme care was required to measure these

differences and that significant changes in the drag could accrue from small changes in the flow. This investigation showed that the drag non-repeatability could be attributed to an increment in the integrated afterbody pressure and that the pressures measured on the tunnel wall varied in sympathy with the afterbody pressures. Since this appeared to be essentially a one dimensional change to the flow at the rear of the test section, it was likely to be attributed to a change in the effective cross sectional area of the tunnel. This paper describes the process of identifying the source of this non-repeatability and the steps taken to rectify the problem.

2   Tunnel Configuration for Half Model Testing

The original design of the ARA 9 ft x 8 ft (2.74 m x 2.44 m) TWT was optimised for complete model testing, using sting mounted models supported from a central vertical strut. The test section has perforated walls with a variable open area ratio, increasing from approximately 5% upstream of the model to a maximum of 22% near the centre of rotation. The tunnel roof has a divergence of 0.3° over the length of the test section to allow for the boundary layer growth on all 4 walls. In order to avoid choking of the flow at high subsonic and supersonic Mach numbers, the tunnel sidewalls diverge by approximately 7° immediately downstream of the test section, opposite the vertical strut leading edge, reducing through a bent wall angle of 6.5° when the strut becomes slab-sided (Fig 1). It should be noted that, although this section comprises only 12% of the main high speed diffuser, future references to the diffuser in this paper will relate to this upstream region.
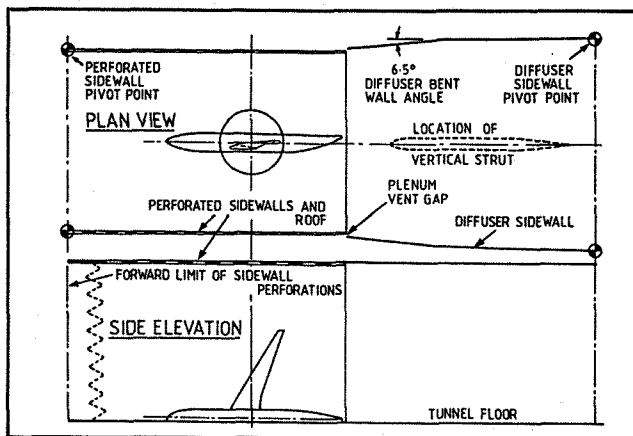

Fig 1   Geometry of the ARA TWT
for Half Model Testing

A zero Mach number gradient in the test section is obtained by very small rotations of the perforated sidewalls about an upstream pivot[†] and the diffuser

sidewalls about a downstream pivot. Differential movement of the perforated and diffuser walls opens a plenum vent gap which creates passive suction through the perforated walls.

For half model testing the model is mounted from the floor of the tunnel, replacing the perforated floor by a solid half model cart which forms a reflection plane in the vicinity of the fuselage. The perforated floor, which is retained close to the tunnel sidewalls, is sealed by a set of plugged plates which extend the reflection plane to the tunnel sidewalls. The vertical support strut is removed from the tunnel to avoid interference with the fuselage afterbody, which means that the initial diffusion angle is larger than the optimum angle. Although it would be possible to change the diffuser bent wall angle manually, this is a slow, labour intensive process and the standard setting for sting mounted models is routinely used for half model testing. The trend towards increasing size of half models results in the afterbody of a large model being close to the rear of the test section and, hence, under the influence of the reduction in Mach number due to the divergence of the diffuser walls (Fig 2). Although this does not normally affect incremental differences between configurations, it does mean that the model will be susceptible to detailed changes in the flow at the rear of the test section.
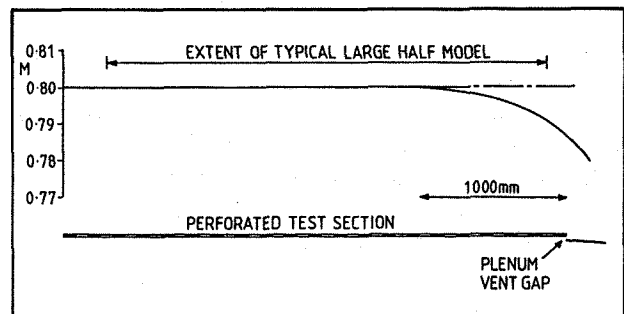

Fig 2   Centreline Mach Number Distribution
for Half Model Testing

3   Thermal Buoyancy in Half Model Testing

The systematic programme of measurements undertaken to confirm that the problem with balance hysteresis had been cured demonstrated surprisingly, but unambiguously, that there was a residual variation in the drag of a half model which was a function of the temperature of the tunnel shell. Fig 3 shows plots of $C_{Do} = C_D - C_L^2/\pi A$, permitting the drag to be plotted at a scale which can discriminate the 1-2 drag count increments

---

[†]The surface curvature is distributed over a length of flexible plate rather than a discrete hinge.
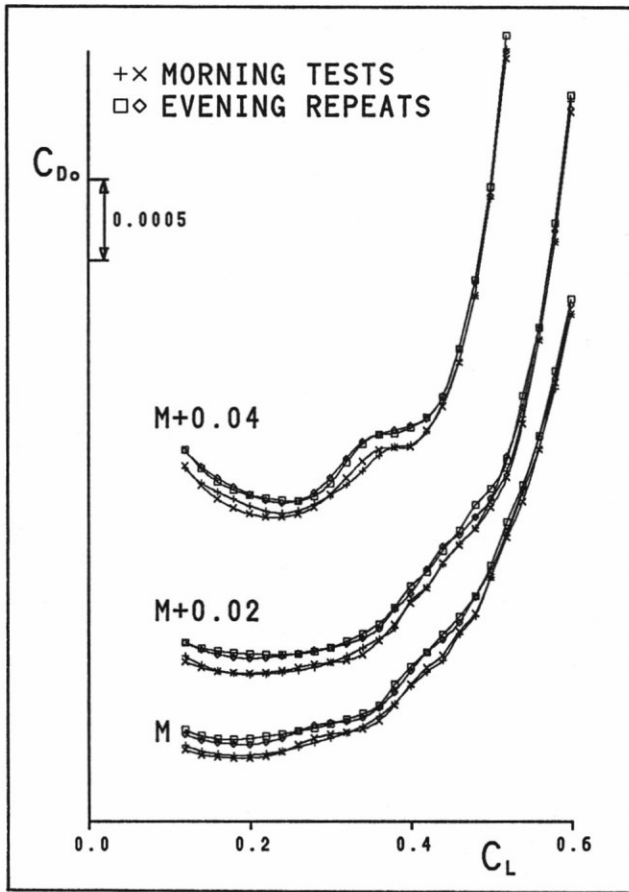
Fig 3 Non-repeatability of Drag Polars
due to Thermal Buoyancy

Of these alternatives, the leak into the plenum was discounted following an exhaustive check of all potential temperature dependent leaks which might admit the required quantity of air into the plenum. Differential expansion of the tunnel shell was also felt to be unlikely after measurements of the tunnel structure temperature indicated that this would change the Mach number distribution by an order of magnitude less than the required effect.

In order to understand the cause of the drag variation, a test programme was undertaken to measure the pressure distribution along the tunnel, using a calibration probe mounted from the floor of the tunnel in the vicinity of a typical half model fuselage (Fig 4). Since these pressures were measured on Scanivalves and the required accuracy in Mach number was 0.0005, it was necessary to use multiple data point averaging to minimise the pressure fluctuations with time. Least squares fits to the average data were used to reduce the influence of the tube signatures of individual pressure tappings which are apparent at the scale shown in Fig 5.
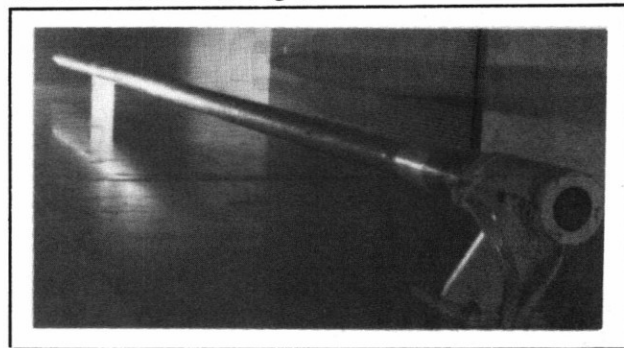
between the results shown. (The shape of the drag polars shown in Fig 3, and subsequently in Figs 15 and 17, has been adjusted to preserve sensitive data whilst maintaining the correct incremental differences between configurations). It was apparent that this difference was due to an aerodynamic change to the tunnel flow since a very small change in pressure could be measured on both the afterbody of the model and the tunnel walls.

Three potential causes of the change in pressure as a function of temperature were identified for further consideration:

- a leak of air into the plenum due to a faulty seal which reduced with increasing tunnel temperature, changing the re-entrant flow from the plenum into the test section
- differential expansion of the tunnel shell, causing a change in the effective cross section of the test section and hence the Mach number gradient
- heat transfer from the air into the tunnel shell, again changing the re-entrant flow from the plenum into the test section.

Fig 4 Half Model Calibration Probe
Installed in the ARA TWT
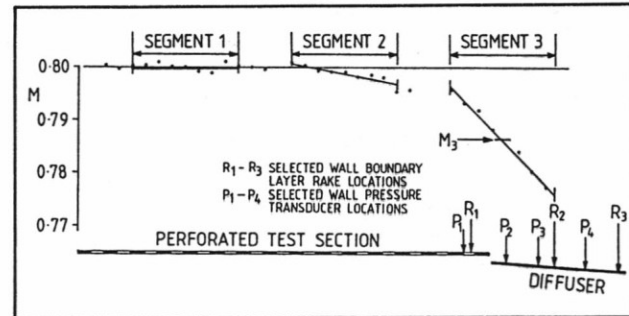
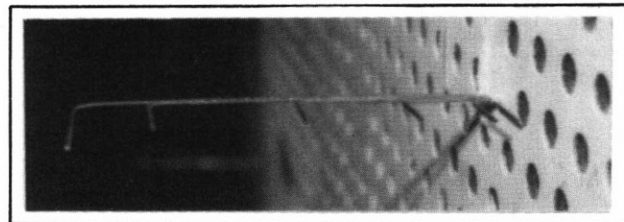**Fig 5** Least Squares Approximation to the
Centreline Mach Number Distribution
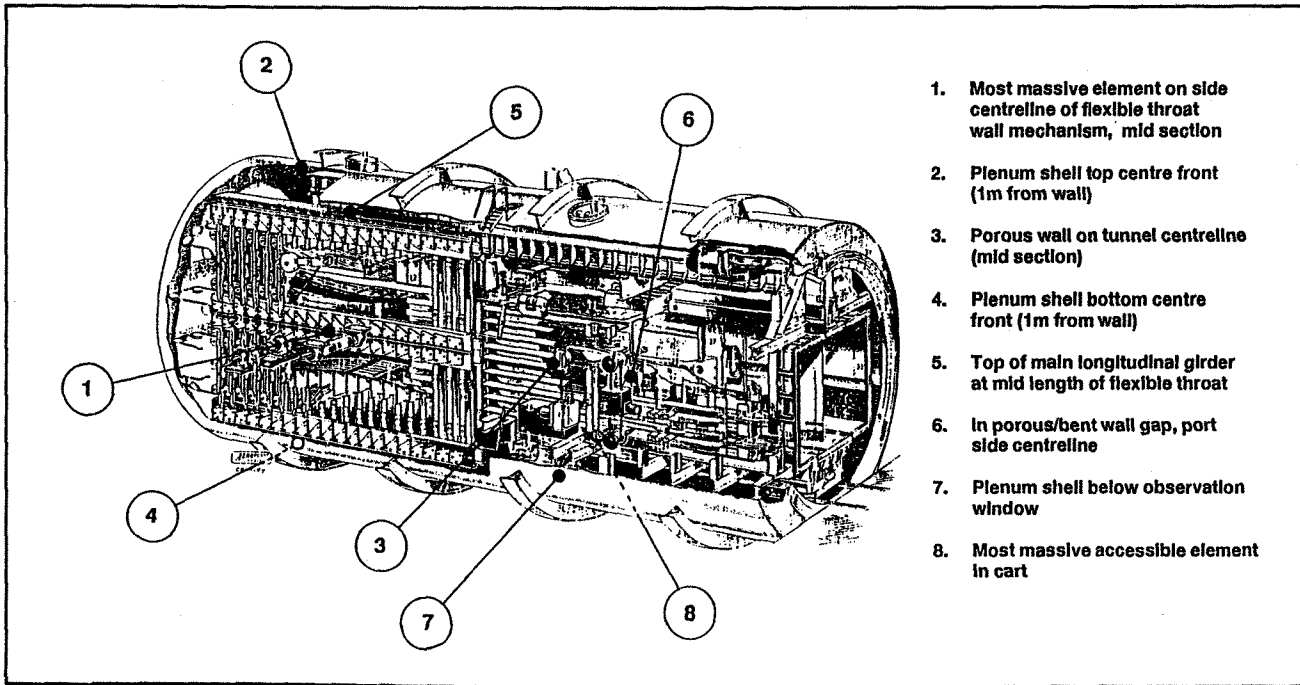

Fig 6 Simple Boundary Layer Rake

Fig 7	**View of Plenum Chamber Showing Thermocouple Locations**

1. Most massive element on side centreline of flexible throat wall mechanism, mid section

2. Plenum shell top centre front (1m from wall)

3. Porous wall on tunnel centreline (mid section)

4. Plenum shell bottom centre front (1m from wall)

5. Top of main longitudinal girder at mid length of flexible throat

6. In porous/bent wall gap, port side centreline

7. Plenum shell below observation window

8. Most massive accessible element in cart

In addition to the centreline probe data, pressures were measured on the walls of the tunnel using both Scanivalves and individual transducers and a large number of simple boundary layer rakes (Fig 6) were installed on the test section and diffuser sidewalls. Finally, eight thermocouples were distributed around the plenum (Fig 7) to measure the relative heating rates of the tunnel structure.

In order to minimise the total number of pressures, the boundary layer rakes measure only 5 pitot tubes and a static pressure. A curve fitting procedure was used, analogous to Coles' Law of the Wall[1,2] for the inner region of the boundary layer combined with a wake-like function for the outer layer, which enabled smooth velocity profiles to be interpolated and consistent boundary layer integrals to be obtained from this small number of measurements within the boundary layer.

The results obtained from the calibration probe broadly confirmed the data which had previously been measured in the half model tests and demonstrated clearly that the temperature sensitivity was due to an aerodynamic phenomenon associated with the tunnel stream. Fig 8 shows the variation through a warm up run of the local Mach numbers derived from the pressure transducers P_1 - P_4 (see Fig 5) and M_3, the mean Mach number measured over segment 3 on the calibration probe. The plenum temperature increment, ΔT, used here is the difference between the free stream stagnation temperature and the value on the plenum shell, thermocouple T7 in Fig 7. Although there is some scatter in the data at the scale plotted, these results show a clear linear trend in which the Mach number reduces with increasing temperature difference after an initial stabilisation at the start of
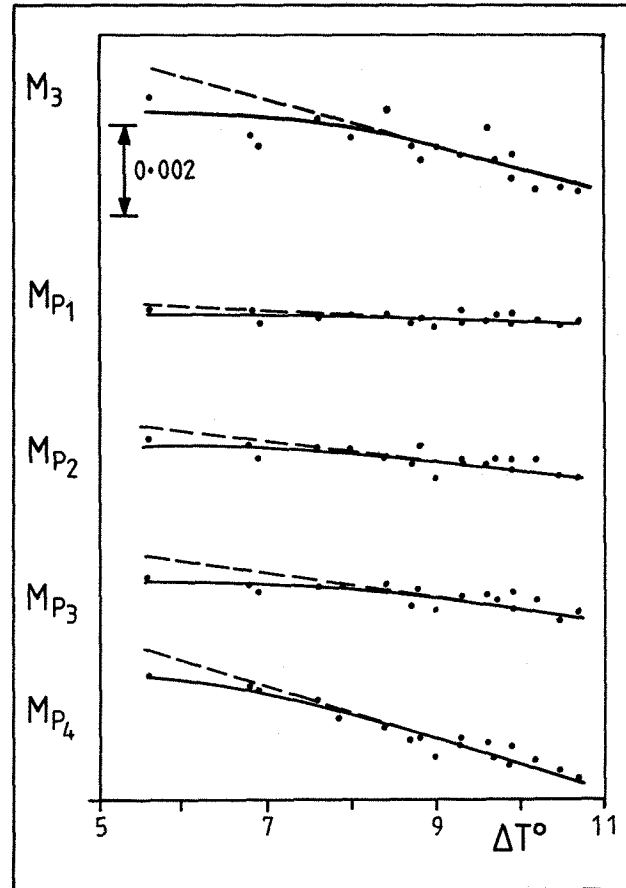

Fig 8	**Variation of Local Mach Number with Plenum Temperature Increment**

2768

the run (low values of ΔT). Since segment 3 of the centreline probe lies opposite transducers P_1 - P_3, a simple one-dimensional effect would imply that M_3 should vary as the mean of M_{P1}, M_{P2} and M_{P3}. This is clearly not the case and the variation at the centreline is somewhat larger, implying a three-dimensional effect in which the conditions at the wall propagate upstream to the centreline. This is similar to the effect of the junction between the perforated wall and the diffuser shown in Fig 5 where the influence of this corner is apparent in the centreline Mach number distribution some distance upstream.
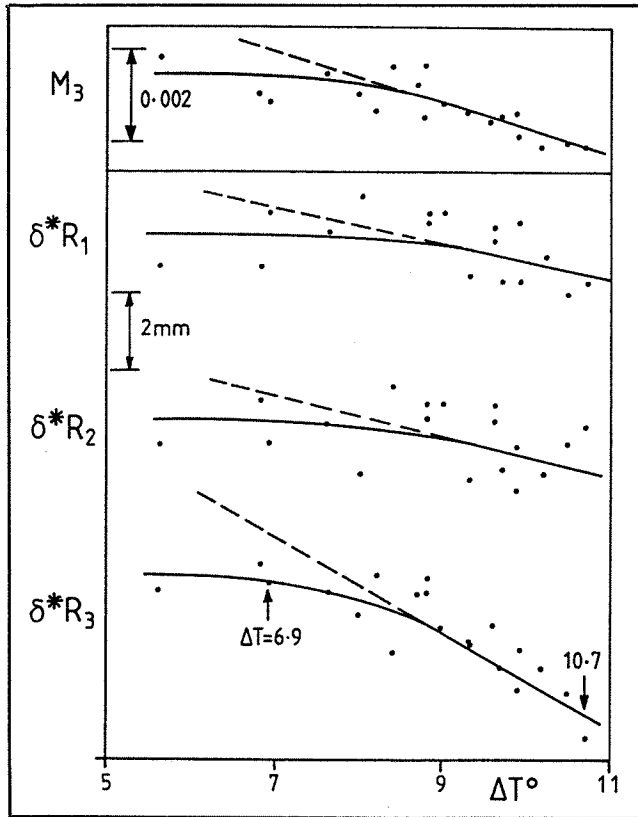

Fig 9 Variation of Sidewall Boundary Layer Thickness with Plenum Temperature Increment
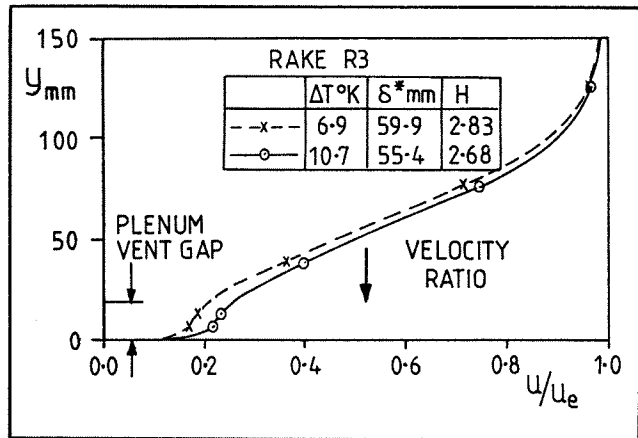

Fig 10 Effect of Temperature Increment on Sidewall Boundary Layer Profile

The reason for the variation in Mach number is immediately apparent from the tunnel wall boundary layer displacement thicknesses shown in Fig 9. Rake R_1 is mounted on the porous wall close to the rear of the test section and rakes R_2, R_3 are on the solid wall just downstream of the test section, as shown in Fig 5. These all show a trend of reducing boundary layer thickness with increasing temperature increment with a similar lag at the start of the run to that found with the local Mach numbers. Fig 10 shows the boundary layer profiles derived for Rake 3 at the two data points indicated on Fig 9. Although Rake 3 is downstream of the region which influences the flow around the model, the results are shown here since they demonstrate the effect of the temperature increment more clearly than the similar, but smaller, differences further upstream. Since these are measured on the diffuser sidewall, downstream of a plenum vent gap, there is an inner layer of very low energy flow for both profiles. An increase in ΔT of approximately 4°K causes a reduction in the boundary layer displacement thickness, δ^*, of approximately 4.5 mm. The difference in velocity profile is most evident in the inner layer, which reduces the shape factor, (δ^*/θ), from 2.83 to 2.68[†]. This finally confirms that the thermal buoyancy can be attributed to heat transfer since a differential expansion of the tunnel would simply cause a very small change in the test section pressure gradient which would not influence the sidewall boundary layer development.

3.1 Heat Transfer Mechanism

Initially, it was expected that the main heat transfer effect would be contributed by the wind-swept surfaces, the perforated walls of the test section. Fig 11 shows that the tunnel walls do indeed respond quickly to a change in the free stream stagnation temperature, both in terms of the initial increase in temperature for the first few minutes after the Mach number has been established and the subsequent linear increase at about 12°/hour once a steady state has been reached. All of the thermocouples in the plenum show an approximately linear variation of 2°/hour

---

[†]The evaluation of δ^* assumes constant stagnation/recovery temperature in the boundary layer outside the sublayer. In fact, the heat exchange in the plenum will reduce the total temperature within the boundary layer, thereby increasing density and further reducing δ^*. This effect is estimated to be an order of magnitude smaller than the observed reduction in δ^*.
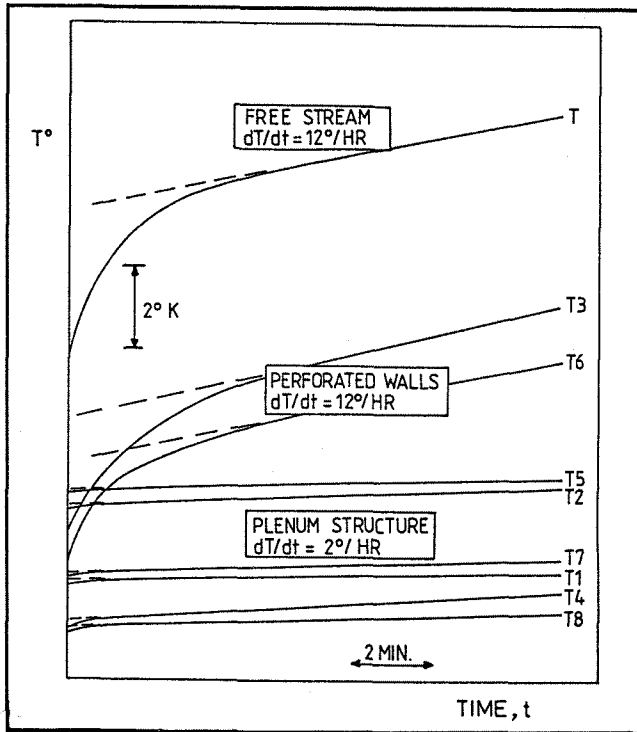
Fig 11 Heating of the Free Stream and the Tunnel Structure
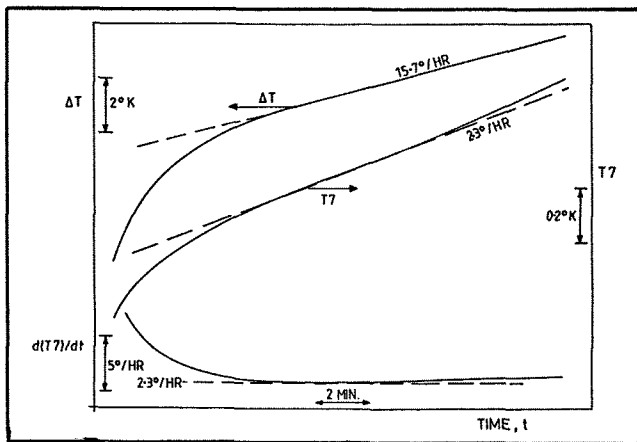

Fig 12 Rate of Change of Temperature of the Plenum Structure

after a very short stabilisation of about 1 minute. However, the perforated walls have a mass of only 2 tonnes, compared with a total of approximately 165 tonnes for the plenum shell and its internal structure. Thus, the internal heat exchange in the plenum chamber dominates that of the perforated walls by a ratio of 14:1 once the linear heating has become established.

The results in Fig 11 are rather disconcerting in that they appear to suggest that, at the start of the run, the increase in temperature of the plenum structure anticipates the temperature difference which causes it. Thermocouple T7 provides a representative mean value of the temperatures measured in the

plenum chamber. Fig 12 shows the rate of change of T7 in finer detail for a warm up run which lasted longer than that used for Fig 11. When the data are plotted at this scale, it is apparent that the variation of T7 with time is consistent with the free stream temperature measurement. Initially, there is a more rapid increase in temperature until the conditions become stable a few minutes after the Mach number has been established. At this point $(d(T7)/dt)$ reaches a minimum. Since $(d(T7)/dt)$ is proportional to ΔT, it starts to increase again and hence the variation in T7 is quadratic. However, the non-linearity in T7 is small and can be approximated by a straight line of increased slope when plotted at the scale shown in Fig 11.
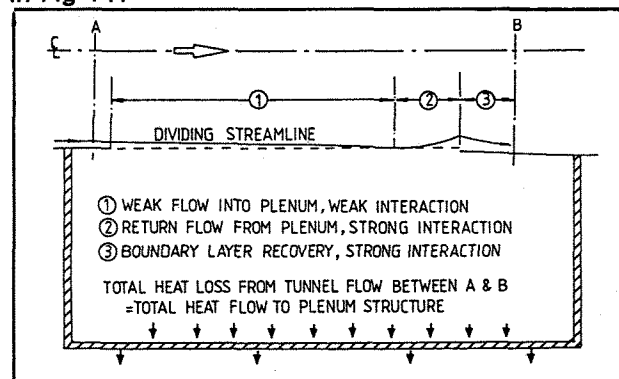

Fig 13 Plenum Mass and Heat Balance in the Empty Tunnel

We are now able to suggest a conceptual model of the heat and mass balance in the plenum chamber, as shown in Fig 13. Upstream of the test section the flow is constrained by a solid wall and the effective stream tube in the tunnel is clearly defined by the wall boundary layer. Over the perforated wall the boundary condition is more complex. The fact that the pressure in the plenum chamber is slightly lower than that in the test section means that there will be a weak transpiration into the plenum over most of the perforated wall (region 1). However, close to the junction between the perforated wall and the diffuser the flow close to the tunnel wall accelerates around the corner to create a local peak suction which creates a strong viscous interaction between the low energy air re-entering from the plenum and the inner layer of the boundary layer which has developed over the perforated wall (region 2). Downstream of the test section the stream is again bounded by a solid wall, but there is a strong viscous interaction associated with the mixing of the tunnel wall boundary layer and the plenum vent flow in the presence of the unfavourable pressure gradient in the diffuser (region 3).

2770

The heat loss from the flow in the test section is balanced by the heat gain in the tunnel structure. Since most of this energy is removed from the air in the plenum chamber, it influences the free stream through the low energy re-entrant flow through the perforated walls of the test section and the plenum vent gap. Since the influence of the re-entrant flow is predominantly close to the wall, there is a disproportionate effect on the boundary layer displacement thickness on the tunnel walls which causes a significant difference to the effective cross sectional area distribution of the free stream. This changes the Mach number distribution in the tunnel in the vicinity of the fuselage afterbody and, hence, changes the streamwise force on the model.

3.2   Rectification of the Thermal Buoyancy Non-Repeatability

Having established thermal buoyancy due to heat transfer in the plenum as a real effect, we now required a procedure to reduce its influence on the measured results. Although the test technique adopted for half model testing tended to minimise the non-repeatability, it was still the source of errors in excess of 1 drag count on occasions. Since the drag variation is a function of the heat loss in the plenum, it is not practicable to measure the fundamental cause of the thermal buoyancy directly. We therefore required a measurement which could be used on a routine basis to correct the data.

Two approaches have been considered to provide a correction in the standard data reduction program. Firstly, it is apparent from the results presented in Figs 8,9 that the drag variation with temperature increment is essentially linear, once stable conditions have been established following a change in Mach number. Hence a calibrated variation of drag with temperature could be used to correct the drag data. Alternatively, since the thermal buoyancy is caused by a change in the Mach number distribution in the vicinity of the afterbody, we could use a measured pressure on the diffuser wall as a basis of the correction.

Part of the technique for accurate drag testing of half models required the use of warm-up runs at the start of the day, particularly during the winter when the temperature difference between the free stream and the tunnel structure was greatest. It was well known that the drag decreased during the course of the warm-up run, but this had previously been attributed to a thermal effect on the balance and was part of the justification of the warm-up run. However, it was now apparent that this drag variation was a real effect of the thermal buoyancy
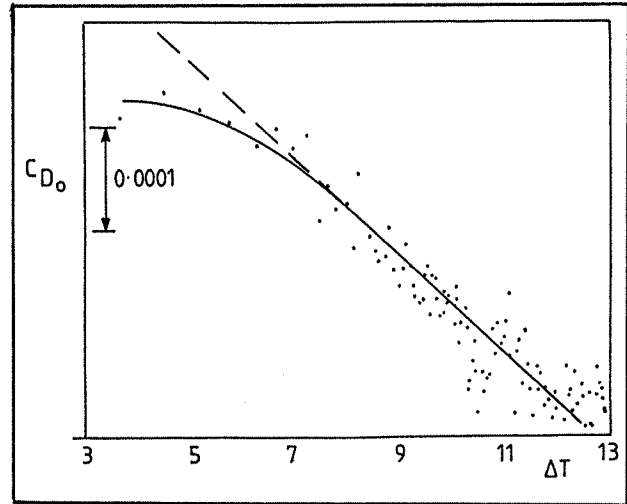

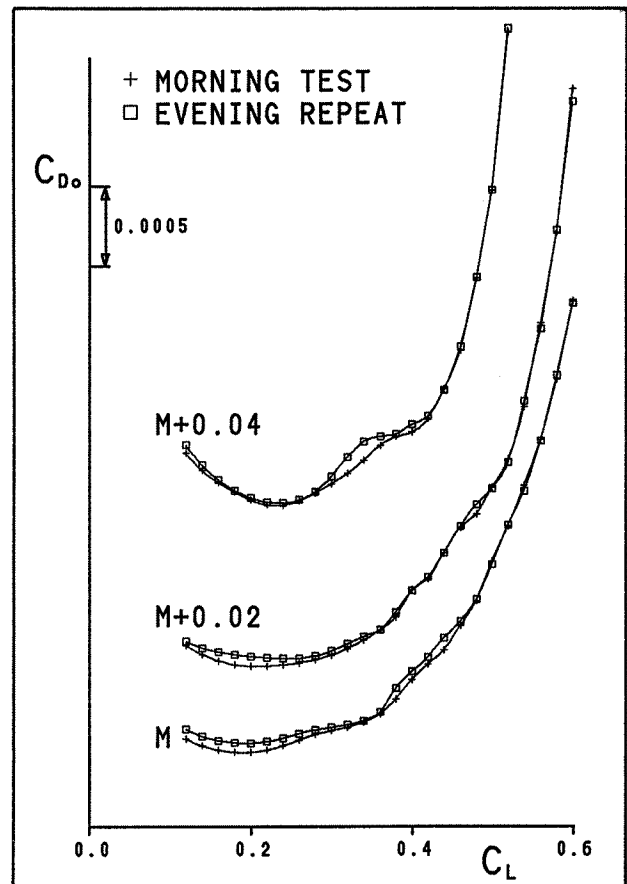Fig 14 Variation of Drag with Plenum Temperature Increment in a Warm Up Run

Fig 15   Residual Non-Repeatability of Drag Polars Using a Temperature Correction

and hence provided a means of calibrating the drag variation with temperature.

Fig 14 shows the variation of drag with the plenum temperature increment during the warm up run preceding the drag polars shown in Fig 3. Once again there is a linear variation of C_{Do} with ΔT after the initial transient, the thermal buoyancy

2771

causing a drag variation of -0.45 counts/°. The drag polars from Fig 3 have been corrected to a common reference value of ΔT and the residual non-repeatability in drag is shown in Fig 15. This provides a significant improvement in the comparison between the two sets of data, with a maximum discrepancy of the order 0.5 drag counts for the three Mach numbers presented.

The procedure which has been adopted to derive a calibration of the drag variation with pressure is based on the observation that the thermal buoyancy is analogous to a pressure leak into the plenum. This can be simulated in a tunnel run by opening a valve in the duct which links the plenum with the high pressure region of the circuit just upstream of the cooler. This permits a bleed of air into the plenum and hence a variation of the re-entrant air through the perforated walls of the test section. Fig 16 shows the variation of drag with diffuser wall pressure obtained from a range of valve settings, providing the basis for a correction of the drag to a specified reference diffuser wall pressure.

The residual non-repeatability of the drag polars following the application of a correction based on the measured diffuser wall pressure is shown in Fig 17. Once again the comparison between the two sets of data is generally satisfactory, with differences of up to 0.5 counts except at the maximum Mach number where the discrepancy is locally of the order 1 drag count.

Half model drag data have routinely been corrected for thermal buoyancy since May 1991 using the diffuser pressure measurements and this has virtually eliminated errors due to temperature variations.

4 Extension of the Test Section for Half Model Testing

Although it proved relatively easy to derive two correction methods to allow for the effect of thermal buoyancy, there remained a concern that the afterbody of a large half model was in a non-uniform flow field (Fig 2) and was subject to potentially large thermal buoyancy corrections. We, therefore, considered ways of extending the test section which would have the potential benefits of providing a longer extent of constant Mach number flow, would improve the shape of the diffuser and would reduce the effect of the thermal buoyancy.

The aerodynamic design of the extended test section was carried out using a modification of a viscous CFD method[3] to model alternative diffuser
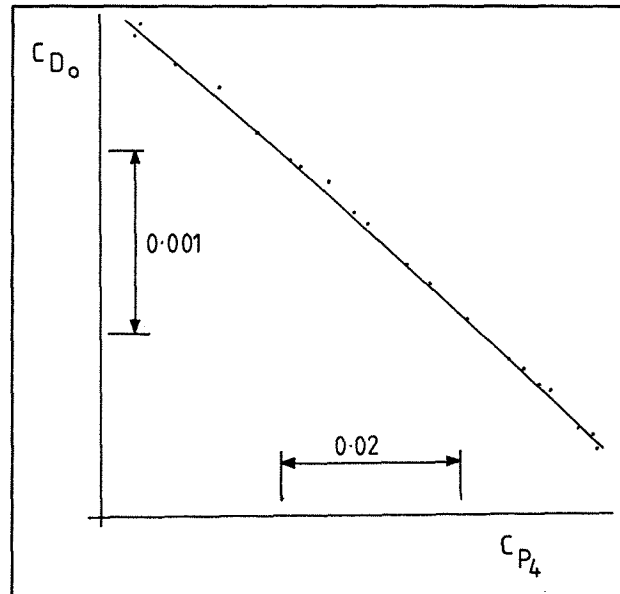

Fig 16   Variation of Drag with Diffuser Pressure Using Plenum Pressurisation
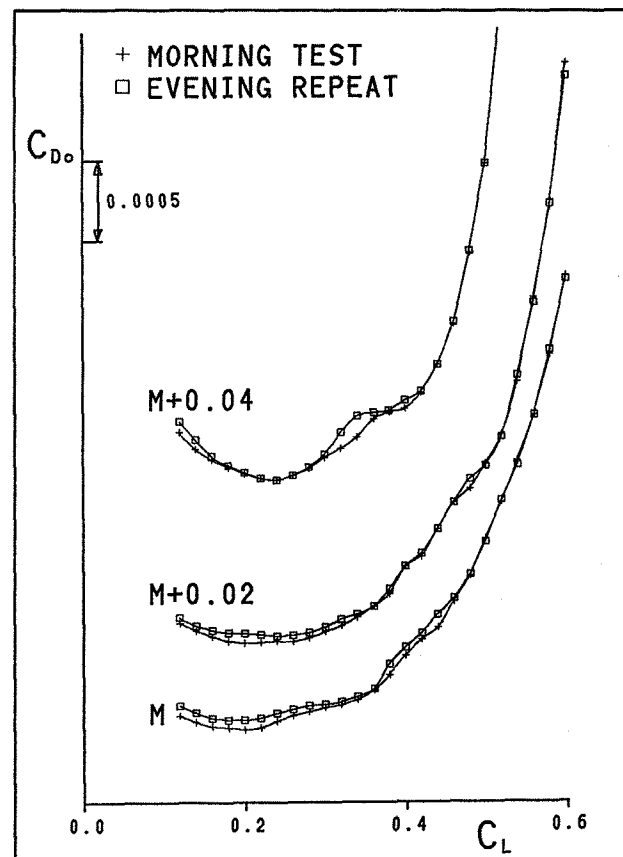

Fig 17   Residual Non-Repeatability of Drag Polars Using a Pressure Correction

shapes in an attempt to obtain a maximum extension of the region of uniform flow in the test section whilst maintaining a satisfactory pressure recovery down the diffuser. Although an attempt was made to represent the transpiration through the perforated wall, it proved difficult to obtain a

converged solution with this modification to the flow solver and the design calculations were carried out using a measured boundary layer at the end of the test section as a starting condition for the viscous code. Some difficulty was also encountered in obtaining a satisfactory grid which permitted a detailed modelling of the high speed flow at the end of the test section and the initial pressure recovery into the diffuser, whilst retaining a momentum balance at the low speeds at the end of the diffuser.
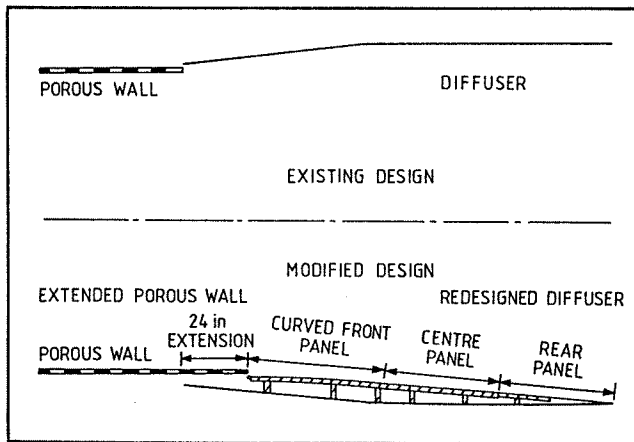

Fig 18   Modifications to the Diffuser for Half Model Testing

The selected design was manufactured using a series of panels which are fitted to the existing perforated walls and diffuser sidewalls, as shown in Fig 18. The perforated walls have been extended by 24 in (610 mm) by mounting a single panel from the longitudinal stiffeners at the back of the existing perforated wall, retaining the movement of the walls which is necessary to optimise the Mach number distribution in the test section.   These extension panels are backed by the existing diffuser walls which have been diverged to provide an air gap depth of approximately 3.2 in (81 mm) which is open to the plenum chamber at its front end. Pressures measured in this gap during the commissioning trials have established that this remains close to plenum pressure for normal test conditions.   The diffuser shape is produced by 3 aluminium skinned, honeycomb panels which fit to the existing diffuser walls.   The front panel is curved to provide continuity in slope between the perforated wall extension and the rear two panels which have a diffusion angle of approximately 5°. Movement of the diffuser wall has been retained, allowing a plenum vent gap to be opened in order to optimise the Mach number distribution in the rear of the test section.

After the redesign of the diffuser, a recalibration of the test section was carried out using the floor mounted calibration probe to reoptimise the tunnel
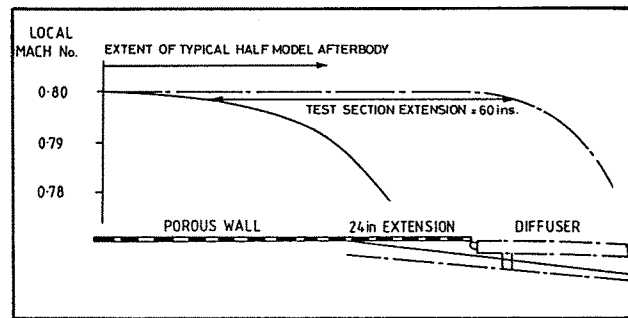

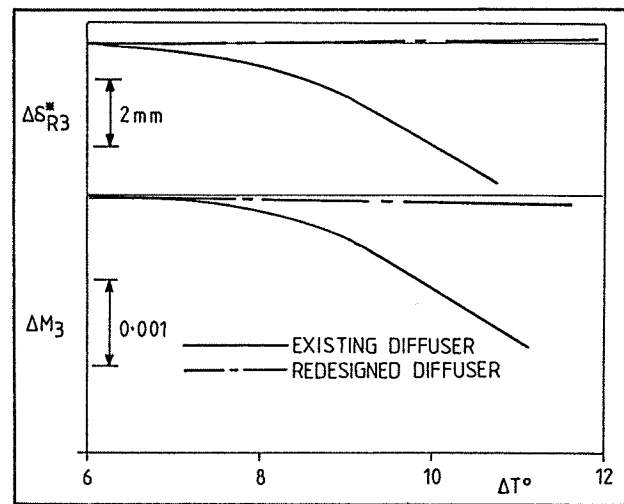**Fig 19   Effect of the Diffuser Modifications on the Centreline Mach Number**

Fig 20   Effect of the Diffuser Modifications on the Thermal Buoyancy in the Empty Tunnel

settings.   Fig 19 shows that, although the perforated wall has only been extended by 24 in, there has been an increase in the effective test section length of approximately 60 in, thus catering for the longest fuselage which is likely to be tested in the ARA TWT. This calibration also showed that the diffuser modifications have reduced the effect of the thermal buoyancy in the empty tunnel.   Fig 20 compares the thermal variation of centreline Mach number and sidewall boundary layer displacement thickness for the existing and redesigned diffusers. Whereas there is a significant thermal effect with the existing diffuser, the redesign shows a negligible influence both on the sidewall boundary layer and the Mach number in the vicinity of the half model afterbody.

Following the encouraging results obtained from the recalibration of the test section, two half models have been tested as part of the evaluation of the redesigned diffuser.   Fig 21 shows a photograph of a typical half model in the TWT with the vertical panels, which form the extended test section and modified diffuser, clearly visible in the background.   Tests have also been carried out using a larger half model as a direct comparison
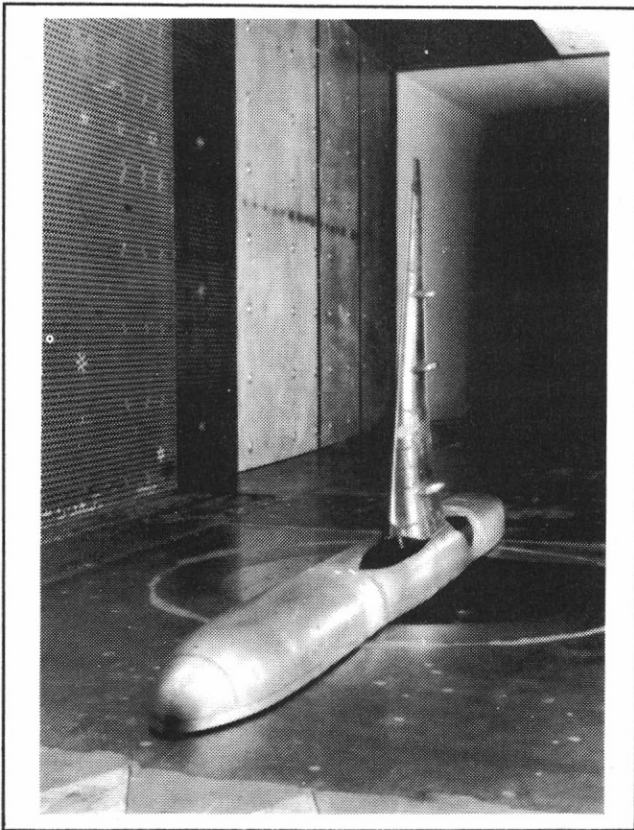
Fig 21   Photograph of a Half Model in
the Extended Test Section

Fig 22 Drag Sensitivity to Temperature During a
Warm Up Run for a Large Half Model

with the same model in the existing tunnel. The results in Fig 22 present the thermal variation of the drag of the large half model for the existing and redesigned diffusers. These confirm that the diffuser modifications have reduced the thermal buoyancy by a factor of approximately 2, although it is apparent that a measurable drag variation with temperature remains for a model in the redesigned diffuser. This appears to contradict the results shown in Fig 20, where the thermal buoyancy was found to be zero in the empty tunnel. The reason for this is thought to be due to the difference in the transpiration into and out of the plenum for the two cases. Having established essentially zero pressure gradient along the test section for the empty tunnel, there is equally only a very small transpiration through the tunnel walls. Hence, although the heat transfer is still present in the plenum, the mechanism by which this is transferred to the tunnel sidewall boundary layer is removed. Since it is the change in the boundary layer displacement thickness which alters the Mach number distribution in the test section, the effect of thermal buoyancy in the empty tunnel is negligible. However, with a model present in the tunnel a transpiration into and out of the plenum occurs as a result of the model blockage. Hence, the mechanism for heat interchange with the sidewall boundary layer is
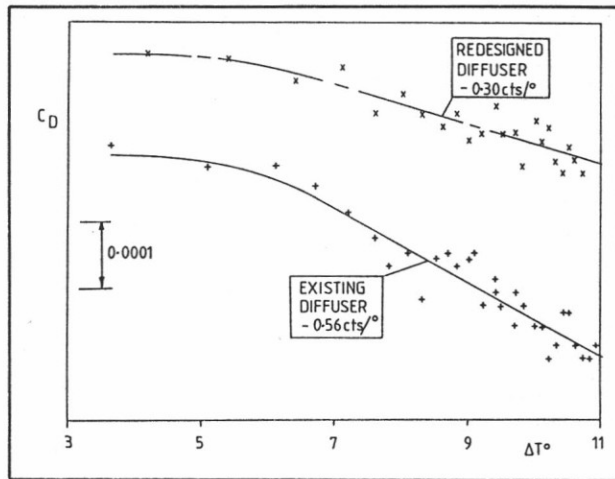
restored and the thermal buoyancy returns. The fact that the test section has been extended means that the re-entrant flow is divorced from the highly viscous region around the plenum vent gap and the magnitude of the thermal buoyancy is reduced compared with the existing test section.

Since thermal buoyancy could still be identified in the drag of a half model installed in the extended test section, a detailed investigation of drag repeatability was carried out using the model shown in Fig 21. Fig 23 shows the drag variation with temperature for this model, obtained from a warm up run in the extended test section. The linear variation of approximately -0.4 drag counts/° is very similar to that which was obtained for this model in the existing test section. This is thought to be due to the fact that, since the model is a more standard size for the ARA TWT, the afterbody is further upstream relative to the perforated wall/diffuser junction. Hence, the drag is less sensitive to the re-entrant flow and its strong interaction with the tunnel wall boundary layer which occurs in the existing tunnel. However, the transpiration through the perforated
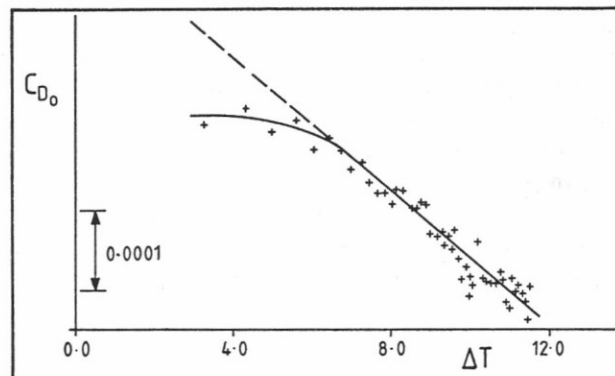

Fig 23 Drag Variation with Temperature During a
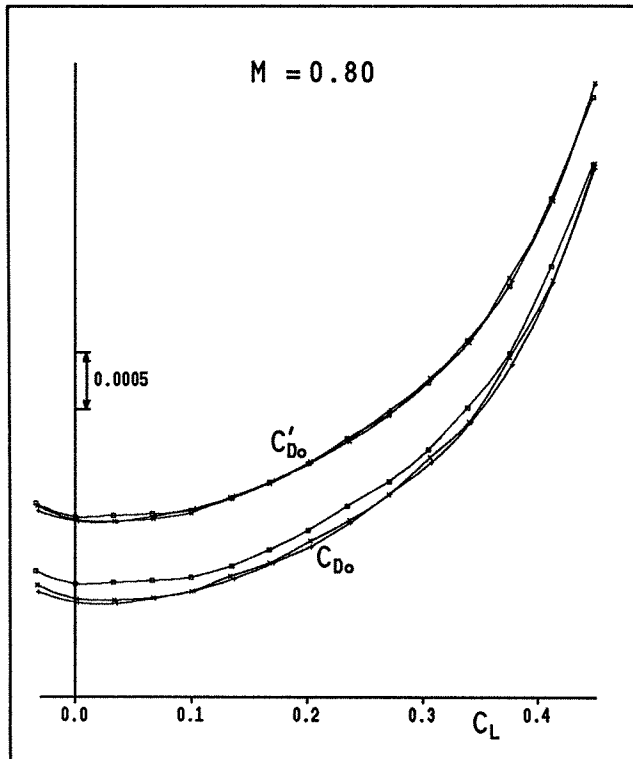Warm Up Run for a Standard Half Model

$M = 0.80$

0.0005

C'_{Do}

C_{Do}

0.0 0.1 0.2 0.3 C_L 0.4

Fig 24 Drag Repeatability in the Extended Test Section With and Without a Thermal Buoyancy Correction

walls into and out of the plenum chamber due to the presence of the model is similar for both the existing tunnel and the extended test section and hence the contribution of the thermal buoyancy to this aspect of the re-entrant flow remains the same in both cases.

Since the purpose of this investigation was to establish the effect of thermal buoyancy on drag repeatability in the extended test section, the tunnel was operated in a way which was intended to generate different thermal conditions in the plenum chamber. This resulted in significant variations in the uncorrected drag polars, $C_{Do} \sim C_L$, shown in Fig 24, with differences between polars in excess of 1.5 drag counts. However, C_{Do}', the drag corrected for thermal buoyancy using the variation obtained from Fig 23, shows very little difference between the polars. The maximum change in corrected drag of less than 0.4 counts provides some encouragement that the drag data from the extended test section are at least comparable and possibly better than the drag standard which has been established for the existing tunnel.

5 Conclusions

During the course of an investigation into a loss of drag repeatability in half model testing in the ARA

TWT, a diurnal variation of drag of up to 2 counts was identified. The cause of this variation has been attributed to a thermal buoyancy due to heat exchange between the tunnel stream and the plenum chamber. Detailed measurements of the conditions in the plenum, the pressures and boundary layer profiles on the tunnel walls and the centreline Mach number distribution have established that the thermal buoyancy can be attributed to a change in the re-entrant flow from the plenum into the rear of the test section. This modifies the inner region of the tunnel wall boundary layer, causing a disproportionate variation in the displacement thickness. This is sufficient to modify the Mach number distribution in the vicinity of a half model afterbody, resulting in a thermal buoyancy in the drag measurements.

An extension of the test section has been designed and commissioned. This has been effective in removing the thermal variation of the tunnel wall boundary layer thickness and the associated change in centreline Mach number in the empty test section. However, the thermal buoyancy remains when a half model is tested in the extended test section, although this is much reduced on a large half model. This has been attributed to the transpiration into and out of the plenum due to the presence of the model, permitting the effect of the heat transfer in the plenum to be transmitted to the sidewall boundary layer. A correction procedure has been developed for both the existing and extended test sections which has virtually eliminated thermal buoyancy as a source of error in the drag measurements, resulting in a drag repeatability of better than 1 count for half model testing in the ARA TWT.

References

1   Coles, D E, 'The turbulent boundary layer in a compressible fluid', ARC 24497, 1963

2   Coles, D E, 'A young person's guide to the data', AFOSR-IFP-Stanford Conference, 1968

3   Peace, A J, 'The calculation of axisymmetric afterbody flows with jet effects by a viscous/inviscid interaction method', ARA Report 67, 1986